

Article

On-Off Control Strategy in a BWRO System under Variable Power and Feedwater Concentration Conditions

A. Ruiz-García * and I. Nuez

Department of Electronic and Automatic Engineering, University of Las Palmas de Gran Canaria, 35017 Las Palmas de Gran Canaria, Gran Canaria, Spain; ignacio.nuez@ulpgc.es

* Correspondence: alejandro.ruiz@ulpgc.es; Tel.: +34-928-451-888

Received: 23 June 2020; Accepted: 3 July 2020; Published: 10 July 2020



Abstract: Although reverse osmosis (RO) is the technology of choice for solving water shortage problems, it is a process that consumes large amounts of energy. Brackish water (BW) desalination is more efficient than seawater desalination due to the lower salinity of the feedwater source. This makes coupling renewable energy sources with BWRO systems attractive. The operation of this type of systems is complex and requires the design of control strategies to obtain optimal operation. The novelty of this work was to propose a simple on-off control strategy for operating a BWRO system that can work with one and two stages and with different configurations considering six spiral wound membrane elements per pressure vessel (PV). The feedwater quality variations of a real groundwater well were used together with a computational tool to simulate the response of the different configurations with the purpose of selecting the most appropriate depending on the input power to the BWRO system. The most suitable configurations were found to be 1:0, 2:1 and 3:2 (PV first stage:PV second stage). It was additionally found that increased feedwater concentrations resulted in shorter operating ranges to maximize permeate water production for the 1:0 and 2:1 configurations, and that the 3:2 configuration was the most suitable for most of the operating range.

Keywords: desalination; reverse osmosis; process control; optimization; variable regime

1. Introduction

Reverse osmosis (RO) is the predominant technology in seawater and brackish water desalination [1]. However, this technology continues to be an intensive energy consumption process [2,3]. Various options can be pursued with the aim of reducing the specific energy consumption (SEC) of RO [4–6], including optimizing the operation of RO desalination plants. Advances in RO membrane technology [7,8] are a key element in the goal of improving desalination efficiency. With respect to spiral-wound membrane modules (SWMMs), studies have been made on the effect of the permeability coefficients on the performance of RO systems in terms of production and solute rejection [9–11]. Significant efforts are being made to try to inhibit the effect of fouling on permeability coefficients during operating time by improving pre-treatment processes [12] and the resistance to fouling [13]. The application of renewable energy sources (RES) to power RO systems has attracted much interest [14]. The operation of RES-driven RO systems is considerably complicated by the problem of variations in power availability and in the characteristics of the feedwater. Given the operational complexity of RO systems and the importance of taking full advantage of technological improvements, it is essential to ensure that desalination plants are working at all times under appropriate operating conditions through efficient and effective process control [15,16].

Models that estimate the behavior of RO systems are crucial when control strategies are applied to this kind of process. I.M. Alatiqi et al. [17] proposed the first multi-loop control system for a seawater

RO (SWRO) process. The RO system had 4-inch hollow-fiber membranes (HFM) (B-10 Permasep from Dupont®), which are not very common nowadays. Plant modeling was carried out using transfer functions, considering feed pressure (p_f) and pH_f as inputs and permeate flow (Q_p) and permeate conductivity ($Cond_p$) as outputs. M.W. Robertson et al. [18] presented an algorithm based on dynamic matrix control (DMC) for the control of an SWRO pilot plant. The process modeling of I.M. Alatiqi et al. [17] was used in this work. J.Z. Assef et al. [19] carried out a study on constrained model predictive control (CMPC) for a brackish water RO (BWRO) desalination unit. The process modeling was done considering four outputs (Q_p , $Cond_p$, trans-membrane pressure and pH_f) and two inputs (rejection flow (Q_b) and inlet acid flow). The goal was to produce a specified Q_p with a desired $Cond_p$, subject to the constraint that pH_f and trans-membrane pressure were within specified bounds. A. Abbas [20] used a DMC algorithm with and without constraints for the control of a simulated SWRO desalination unit with HFM. The dynamic model used in their work was based on transfer functions and developed in a previous study by other authors [17]. A control system design for RO systems using advanced optimization techniques was proposed by A. Gambier et al. [21]. Trans-membrane pressure and pH_f were considered as inputs, and Q_p and $Cond_p$ as outputs in the transfer function-based model. A.R. Bartman et al. [22] designed and implemented a nonlinear model-based control system for a pilot-scale BWRO desalination plant. The model [23] used was based on a mass balance taken around the entire system and on an energy balance taken around the actuated concentrate valve. The model proposed by M.W. Robertson et al. [18] was implemented by G. Kim et al. [24] in an optimization algorithm with an immune-genetic approach to obtain the parameters of a proportional-integral-derivative (PID) controller. The previously mentioned mass/energy-based model proposed by C.W. McFall et al. [23] was used by A.R. Bartman et al. [25] in a simulated BWRO system with concentrate recirculation. In a later work, A.R. Bartman [26] minimized the *SEC* of an SWRO system (18 pressure vessels (PVs) each with 6 SWMMs in series) through a non-linear optimization model. A robust model-based control for an RO desalination unit with tubular membranes was proposed by M. Al-haj Ali et al. [27]. The three-parameter nonlinear Spiegler–Kedem model was used in this work. The same model was used by A. Emad et al. [28] in a periodic control work in a tubular RO process. A. Gambier [29] designed a robust PID controller using a multi-objective normal boundary intersection algorithm. A pilot BWRO desalination plant for tap water purification was used. The model of the aforementioned plant was simplified to a single-input single-output (SISO) system, where input was the RO concentrate valve position and output the permeate flow. M.M. AlDhaifallah et al. [30] designed a PID controller for a simulated SWRO system with HFMs using the solution-diffusion model. D. Li et al. [31] proposed a cascade control system for a simulated RO system with SWMMs. The models (steady state and dynamic) used had previously been proposed by T. Zhao et al. [32], and were based on solution-diffusion, mass balance and momentum balance. S. Sobana and R.C. Panda [33] studied model-based controls in a simulated SWRO system taking into consideration servo and regulatory problems. The model was based on transfer functions and the outputs were Q_p , permeate concentrate (C_p) and pH_f and the inputs p_f and flux recovery R . A modified PID control with H-infinity loop shaping synthesis for simulated RO systems was proposed by B.D.H. Phuc et al. [34]. A transfer function model was obtained for the RO system considering angular pump speed and RO concentrate valve position as inputs and Q_p and C_p as outputs. In a later work [35], the same authors carried out a dynamical analysis and control synthesis for RO systems against water hammering. In this case, a dynamical model based on a macroscopic kinetic energy balance and irreversible thermodynamics previously developed by A.R. Bartman et al. [25] was used. V. Feliu-Batlle et al. [36] used a transfer function-based model to propose a fractional order controller for a SWRO system. The dynamics of the system were experimentally identified. A control system comprised of two loops, the first using a loop-shaping design method and the second a super-twisting sliding mode control, was proposed by M. Zebbar et al. [37]. The RO system model was based on mass and energy balances. An implementation of an expert model predictive controller in a pilot BWRO and SWRO system was carried out by R. Rivas-Perez et al. [16]. The expert controller included an

identification block with on-line calculation of the parameters of the prediction model. The model for the RO systems was based on transfer functions. W. Khiari et al. [38] proposed a power control strategy for a BWRO desalination plant powered by an isolated hybrid photovoltaic/wind source without battery. A solution-diffusion model was used for the RO process. Experimental work was done to determine performances under different operating conditions in the safe operating window (SOW). Different feedwater concentrations were considered (2, 4 and 6 g L⁻¹) and R was limited to 20%. The proposed control system allowed operation of the BWRO desalination plant for a wide range of power variations. Most of the aforementioned works used process modeling based on transfer functions or more precise models without experimental validation.

Under normal conditions, BWRO is more efficient than SWRO desalination due to the difference in the osmotic pressure of the feedwater solutions. This makes the use of RES an attractive option to power BWRO desalination systems. The composition of groundwater, one of the main feedwater sources tends to fluctuate as the result of variations in different factors (temperature, rainfall, agricultural irrigation, etc.) [39,40]. Significant fluctuations in osmotic pressure may occur that can affect the performance of BWRO systems. Several authors have studied RES-powered BWRO systems. S.M. Hasnain and S.A. Alajlan [41] studied a BWRO system powered by photovoltaic energy using real groundwater. A pilot plant was used and the study focused on cost assessment without providing operating data. W. Gocht et al. [42] used a pilot BWRO desalination plant with a Q_p capacity of 40 m³ d⁻¹. A. Schäfer et al. [43] carried out a performance analysis of a photovoltaic-powered hybrid BWRO membrane system considering variations in feedwater salinity. The RO system only had one membrane element and SEC variations of between 5.5 kWh m⁻³ at a feed concentration of 1 g L⁻¹ salt and 26 kWh m⁻³ at a feed concentration of 7.5 g L⁻¹ salt were reported. The same research group [44,45] continued their study by evaluating the effect of energy fluctuations and feed salinity on the performance of a small single-stage BWRO system. The SEC and permeate quality were evaluated for different membranes along 12 h of operation. M. Khayet et al. [46] carried out an interesting work based on the optimization of a solar-powered BWRO system with a Q_p capacity of 0.2 m³ d⁻¹ for drinking water. A synthetic solution of 6 g L⁻¹ NaCl was used as feedwater in the aforementioned small single-stage plant. Runs of 2 h were done providing operating data in terms of production, salt rejection and energy. The authors concluded that the optimized RO plant could guarantee potable water production with a SEC from 1.2 to 1.3 kWh m⁻³. H. Quiblawey et al. [47] analyzed the performance of a small, single-stage photovoltaic-powered BWRO desalination plant to produce 0.5 m³ d⁻¹. The variation of R and salt rejection with temperature and the increase of SEC when R decreased were reported. H. Cherif and J. Belhadj [48] evaluated a hybrid photovoltaic-wind system to produce desalinated water from a BW source. The BWRO desalination plant design was based on software simulation (ROSA software from Dupont®). The first stage had 4 PVs, each with 4 SWMMs, and the second stage 4 PVs, each with 2 SWMMs. G.L. Park et al. [49] studied the effect of wind speed fluctuation on the performance of an RES-powered BWRO plant comprised of one 4-inch diameter SWMM element. They used synthetic solutions of NaCl (2.75 and 5.5 g L⁻¹) as feedwater in a system with a Q_f capacity of 0.3 m³ h⁻¹. Similarly, B.S. Richards et al. [50] considered the effect of real wind fluctuation and energy buffering on the performance of a BWRO pilot plant in terms of Q_p , C_p and SEC . The same group continued this research line considering a small single-stage BWRO system unit, studying a safe operating window methodology using a new and old SWMM [51] and the influence of solar irradiance fluctuation on plant performance [52]. Most of the studies that have been undertaken have only considered small size (pilot-scale or lab-scale) single-stage BWRO system configurations which differ considerably from full-scale BWRO systems that commonly have at least two stages and 4 SWMMs per PV [5,53].

The aim of this work was to evaluate through an on-off control strategy the different SOWs of a simulated BWRO system using the real feedwater fluctuation characteristics of a groundwater well that has been under study for 10 years. The BWRO system has three PVs in the first stage and 2 PVs in the second stage. Depending on the power input and C_f in the BWRO system, the control

system established a BWRO system configuration to maximize Q_p . A computational tool validated in a previous work by the authors [53] was used to simulate the behavior of the BWRO systems under different operating conditions.

2. Methodology

2.1. Feedwater Characterization

The feedwater source (groundwater well) is located on the island of Gran Canaria (Canary Islands, Spain), with coordinates latitude $27^{\circ}50'52.04''$ N, longitude $15^{\circ}29'00.20''$ W, and an elevation of 160 m above mean sea level. The feedwater characteristics as well as how the samples were collected and analyzed have been published by the authors in a previous work [54]. The well was monitored for 10 years, taking two or three samples per year. Table 1 shows the feedwater characteristics in terms of pH, T and inorganic composition. The total dissolved salts (TDS) content was considered as the sum of the analyzed ions and not the measurement of TDS itself as not every single ion was analyzed. The highest TDS were found in sample 11 ($5815.20 \text{ mg L}^{-1}$) and the lowest in sample 20 ($1218.79 \text{ mg L}^{-1}$). The silt density index (SDI) was assumed to be between 2 and 3, as is usual for this type of water after a $5 \mu\text{m}$ microfiltration stage [55].

Table 1. Feed water inorganic composition in mg L^{-1} .

Sample	pH	HCO_3^-	Cl^-	SO_4^{2-}	NO_3^-	Na^+	K^+	Ca^{2+}	Mg^{2+}	Fe^{2+}	SiO_2	TDS	T
1	7.05	175	2620	165	7.9	400	29	474	475	0.6	60.5	4407.00	25.20
2	6.94	155	2500	180	5.3	422	38	532	383	0.2	36	4251.50	25.60
3	7.37	175	2650	168	5.3	450	30	561	406	0.15	55.7	4501.15	25.00
4	7.48	100	2420	192	5.7	307	30	512	409	0.11	53.4	4029.21	25.10
5	7.24	122	1715	150	6.9	257	28	368	292	0.09	52.5	2991.49	24.90
6	7.27	216	2230	323	9.6	369	30	480	399	0.1	65	4121.70	25.50
7	7.05	190	3180	306	3	458	17	783	483	0.35	57	5477.35	25.30
8	7.05	167	2418	175	6	451	29	660	264	0.5	57	4227.50	25.00
9	7.03	92	2680	166	4.3	339	35	605	428	0.13	30	4379.43	24.80
10	7.46	287	2684	196	1	720	48	432	370	0.09	59	4797.09	25.40
11	7.10	304	3362	180	2.2	830	85	566	453	1	32	5815.20	25.70
12	7.10	305	3360	180	2	828	83	570	450	0.8	30	5808.80	25.00
13	7.40	184	2420	182	1.4	324	32	570	390	0.27	56.3	4159.97	25.20
14	7.10	185	2872	200	5	383	28.9	594	505	0.48	55.8	4829.18	25.10
15	7.80	155	2610	209	0.5	399	38.1	645	405	0.21	92.9	4554.71	25.00
16	7.40	152	2966	273	12.9	469	33.6	600	504	0.19	54.5	5065.19	24.80
17	6.90	260	3023	218	5	425	36.9	632	552	0.08	54.7	5206.68	24.60
18	7.70	173	2930	253	6.8	410	17	620	504	0.14	46	4959.94	25.70
19	7.00	170	2758	232	7.2	363	38.2	669	546	0.15	50.8	4834.35	25.50
20	7.60	215	484	85.6	13.6	208	11.7	76.8	78.1	0.094	45.9	1218.79	25.00
21	8.04	193	1831	150	8.36	468	22.5	395	323	0.17	52.1	3443.13	25.50
22	8.19	197	1715	148	8.1	622	28.6	423	308	0.11	34.2	3484.01	25.20
23	7.72	227	654	108	6.73	214	15.6	120	88.5	1.21	66.6	1501.64	25.10
24	7.58	196	2259	152	74.8	354	35.1	465	418	1.22	62.3	4017.42	25.00

2.2. Bwro Desalination System

The BWRO system considered for this study has 3 PVs in the first stage and 2 PVs in the second stage (3:2) and is shown in Figure 1. Six SWMMs per PV were considered along with a FILMTEC™ membrane module. The BW30-400 computational tool used was validated with experimental data of full-scale BWRO desalination plants with the aforementioned SWMMs installed [53]. In the cited study, the purpose of the computational tool had been to provide optimal BWRO designs. In the present study, this tool is used to simulate the operating windows of the different configurations under different C_f . PVs of 6 SWMMs were considered as this is a typical PV size [53]. Valves 1 to 6 allowed the configuration of the BWRO system to be changed depending on the feedwater solute concentration

and the input power (P_{in}) to the system. Non-return valves have to be installed (not shown in Figure 1) to avoid reverse flow to PVs that are in off position. The P_{in} , supplied by the high pressure pump (output power of the high pressure pump) is a manipulable variable that depends on Q_f and p_f set by the variable frequency drive of the high pressure pump. Another manipulable variable is R through the reject flow which depends on the on/off percentage of the RO concentrate valve. Specific high pressure pumps and their performances were not considered in this study. The different configurations that could be established were 1:0, 2:0, 3:0, 2:1, 3:1 and 3:2. For each P_{in} and system configuration, the operating point that provided maximum production was selected as the use of RES to power the BWRO system was assumed. Most BWRO desalination plants in Gran Canaria are used for agricultural irrigation purposes so no permeate quality restrictions were added.

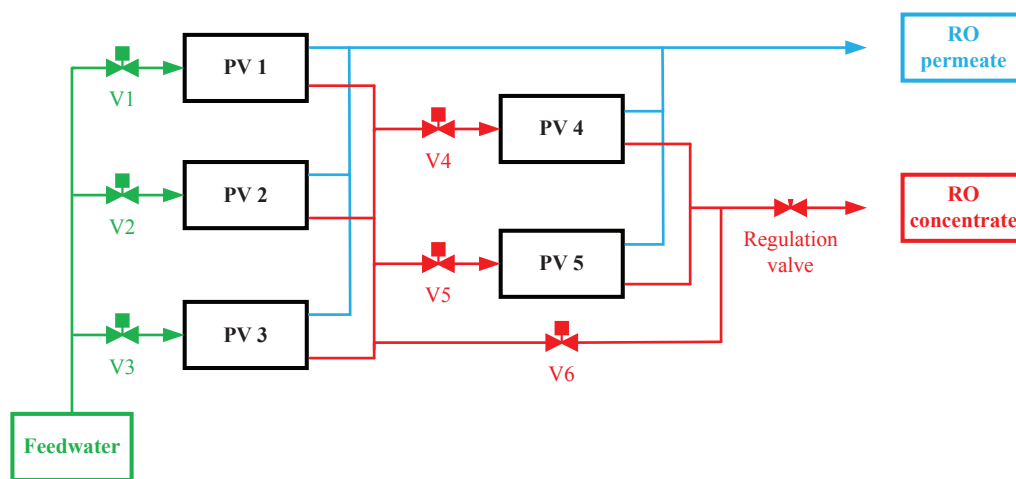


Figure 1. Brackish water reverse osmosis (BWRO) desalination system.

2.3. Process Modeling

The solution-diffusion transport model [56,57], which presumes that the RO membrane does not have porous or imperfections, was utilized. This model is based on considering that each solvent and solute are dissolved in the membrane separately on the feed-brine side and then diffused in individual fluxes through the membrane under the effect of pressure and concentration gradients. This is the most extended model and provides results close to the real behavior of RO systems for both seawater and brackish water [58]. The mentioned transport model was implemented in the algorithm [53] as it usually provides results close to the real behavior of these systems. The transport equations used mean membrane element values, and permeate pressure drops as well as T changes along the RO system were disregarded. The calculation algorithm considers some simplifications that have been detailed in a previous work [53]. Figure 2 shows the inputs and outputs of the calculation algorithm considering the constraints established by the membrane manufacturer (maximum permeate flow (Q_{p-max}), minimum rejection flow (Q_{r-min}) and maximum feed flow (Q_{f-max}). One of the main limiting factors in BWRO desalination is the presence of poorly soluble compounds in the feedwater that can cause scaling. As a result, antiscalant products are commonly used in BWRO desalination plants to avoid the problems caused by scaling and increase the maximum flux recovery (R_{max}). R_{max} depends, amongst other things, on the type of antiscalant that is used. The calculation algorithm has a specific function (R function) where R_{max} is calculated for various antiscalants [59]. The aforementioned algorithm provides the possible operating points in accordance with the considered constraints and BWRO system configurations. With the inputs, the algorithm calculates the outputs considering the mean operating parameter values per SWMM. The calculation algorithm assumes a negligible pressure decrease on the permeate side, constant pressure drop along the membrane elements on the feed-brine side, constant permeate flow per membrane element, constant feed-brine concentration (C_{fb_i}) on the

membrane surface (C_{m_i}) and constant membrane element feed pressure (p_{f_i}). Equations (1) and (2) [60] were used to determine the outputs of the BWRO system.

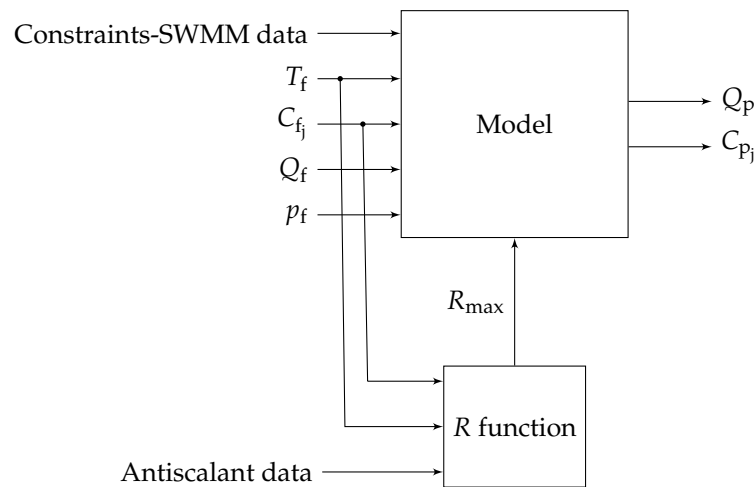


Figure 2. Inputs and outputs of the calculation algorithm.

$$Q_p = \sum_i^n Q_{p_i} = \sum_i^n \left(A \cdot TCF \cdot FF \cdot S_{m_i} \cdot \left(p_{f_i} - \frac{a \cdot \left(\frac{Q_{f_i} + Q_{r_i}}{2} \right)^b \cdot 0.07}{2} - p_{p_i} - 0.0787 \cdot (273 + T) \cdot (\Sigma m_j)_f \cdot \frac{C_{f_i} + C_{b_i}}{C_{f_i}} \cdot e^{0.7 \cdot \frac{Q_{p_i}}{Q_{f_i} + Q_{r_i}}} + 0.0787 \cdot (273 + T) \cdot (\Sigma m_j)_p \right) \right) \quad (1)$$

$$C_{p_j} = B_j \cdot e^{0.7 \cdot \left(\frac{Q_{p_j}}{Q_{f_j} + Q_{r_j}} \right)} \cdot TCF \cdot \frac{S_m}{Q_{p_i}} \cdot \frac{C_{f_j} \cdot \left(1 + \frac{1}{1 - \frac{Q_p}{Q_f}} \right)}{2} \quad (2)$$

If $T \geq 25 \text{ }^\circ\text{C}$:

$$TCF = \exp \left[2640 \cdot \left(\frac{1}{298} - \frac{1}{273 + T} \right) \right] \quad (3)$$

If $T \leq 25 \text{ }^\circ\text{C}$:

$$TCF = \exp \left[3020 \cdot \left(\frac{1}{298} - \frac{1}{273 + T} \right) \right], \quad (4)$$

where Q_p is the permeate flow of the RO system, i is the membrane element (1... n), n is the number of membrane elements in series, Q_{p_i} is the permeate flow of the membrane element i , A is the average water permeability coefficient of the membrane, TCF is the temperature correction factor, FF is the fouling factor (considered = 1, new SWMMs), S_{m_p} is the membrane area, a and b are two parameters obtained experimentally to calculate the pressure drop, p_{p_i} is the permeate pressure (considered as 5 psi), T is the feed temperature, m is the molal concentration of each ion j , C_b is the concentration in the brine, B is the average ion permeability coefficient of the membrane. The p_f range considered was between 7 and 20 bar in steps of 0.5 bar, and the Q_f range between $Q_{r\text{-min}}$ and $Q_{f\text{-max}}$ in steps of $10 \text{ m}^3 \text{ d}^{-1}$.

3. Results and Discussion

Figures 3 and 4 show the different SOWs considering the different BWRO configurations (1:0, 2:0...) and two different C_f (1.2 and 5.8 g L^{-1} , respectively). The irregularities in the contours of the surfaces are due to the p_f and Q_f steps. It can be observed that with lower C_f there is greater separation along the x-axis between the different SOWs. This is because low osmotic pressure of the

feed solution allows water production with low P_{in} , which can result in SWMMs operating outside their recommended range (in terms of Q_{r-min}) due to the very high permeate production of the first SWMMs. Figure 3 shows a possible operating range for the 1.0 configuration at very low P_{in} . However, the 2:0, 3:0 and 3:1 configurations can be discarded, as higher permeate productions can be attained with the 2:1 and 3:2 configurations with the same P_{in} . The same occurs when considering higher C_f (Figure 4), although in this case the operating range of configuration 1:0 is shorter. Having higher C_f means higher osmotic pressure and a lower number of operating points that are outside the recommended range. This is because the first SWMMs do not produce a high amount of permeate due to osmotic pressure, resulting in the subsequent SWMMs remaining within the recommended range since, as we move along the PV, the SWMMs produce less permeate flow. For the solution with higher C_f , operating conditions with higher P_{in} were found to be suitable as higher osmotic pressure allows the BWRO system to remain within the SOW. However, the energy required is also higher and production is decreased compared to the case with lower C_f . It can be appreciated how permeate production of more than $700 \text{ m}^3 \text{ d}^{-1}$ can be obtained with sample 20 as feed solution (Figure 3), whereas, with sample 11 as feed solution, permeate production is below $600 \text{ m}^3 \text{ d}^{-1}$ and more energy is required. The SOWs are affected by SWMM characteristics such as S_m or permeability coefficients. As a result of changes in these characteristics, there is a shift in the SOWs and, consequently, in the optimal operating points.

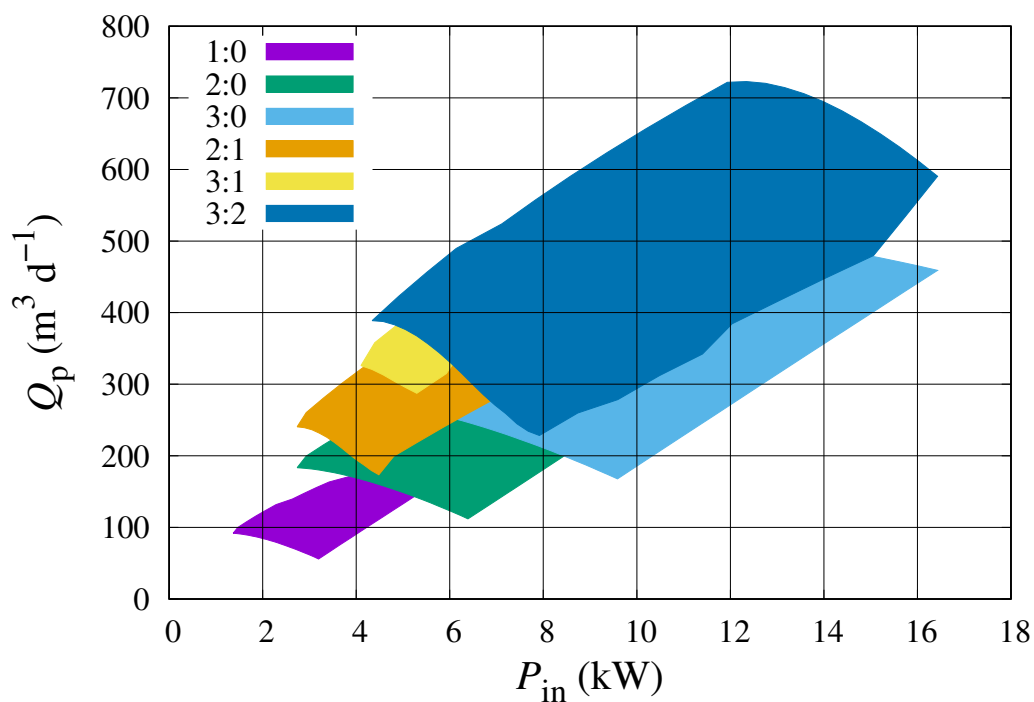


Figure 3. Permeate production for different BWRO configurations using sample 20 (Table 1) as C_f .

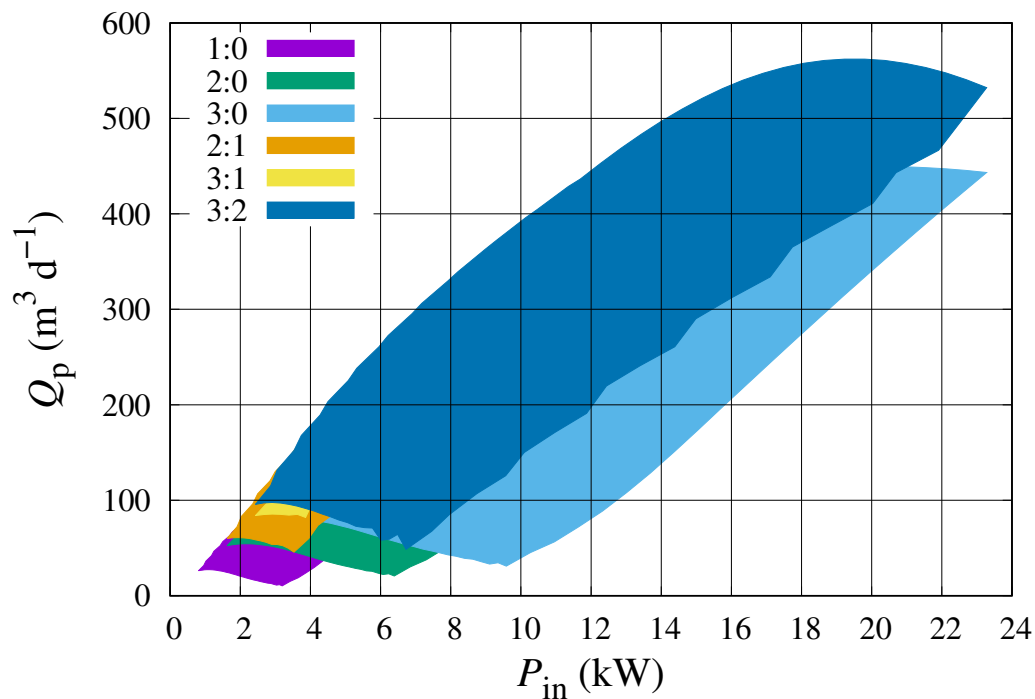


Figure 4. Permeate production for different BWRO configurations using sample 11 (Table 1) as C_f .

Figures 5 and 6 show the R for the most relevant BWRO system configurations (1:0, 2:1 and 3:2), considering the C_f of samples 20 and 11, respectively. A wider operating range can be observed for configuration 3:2. This is due to the higher number of SWMMs allowing more possible operating points without exceeding the membrane manufacturer constraints. Higher R values were obtained for the configurations with two stages as more SWMMs are arranged in series in this sort of configuration. While the highest R can be attained with both the 2:1 and 3:2 configurations, the 2:1 configuration requires less input power but has a lower production than the 3:2 configuration (Figure 3). The highest R value attained with a single-stage configuration was around 60%. Considering as C_f a feed solution with higher TDS_f (5.82 g L^{-1}), the surfaces of the three configurations considered are closer together, as observed previously (Figure 4). The change in feedwater inorganic composition results in a decrease in R_{\max} . With higher TDS_f , the difference in terms of R between the single- and two-stage configurations is lower. It should be mentioned that, in terms of production, the 2-stage configurations outperform the others as more SWMMs are arranged in series and so more elements are producing permeate. The influence of TDS_f (and therefore of π) can be observed by comparing Figures 5 and 6. With the 3:2 configuration and a P_{in} of 8 kW, an R of about 77% can be observed in Figure 5 compared to a value of about 64% in Figure 6. Naturally, this also affects the production of the system and its efficiency.

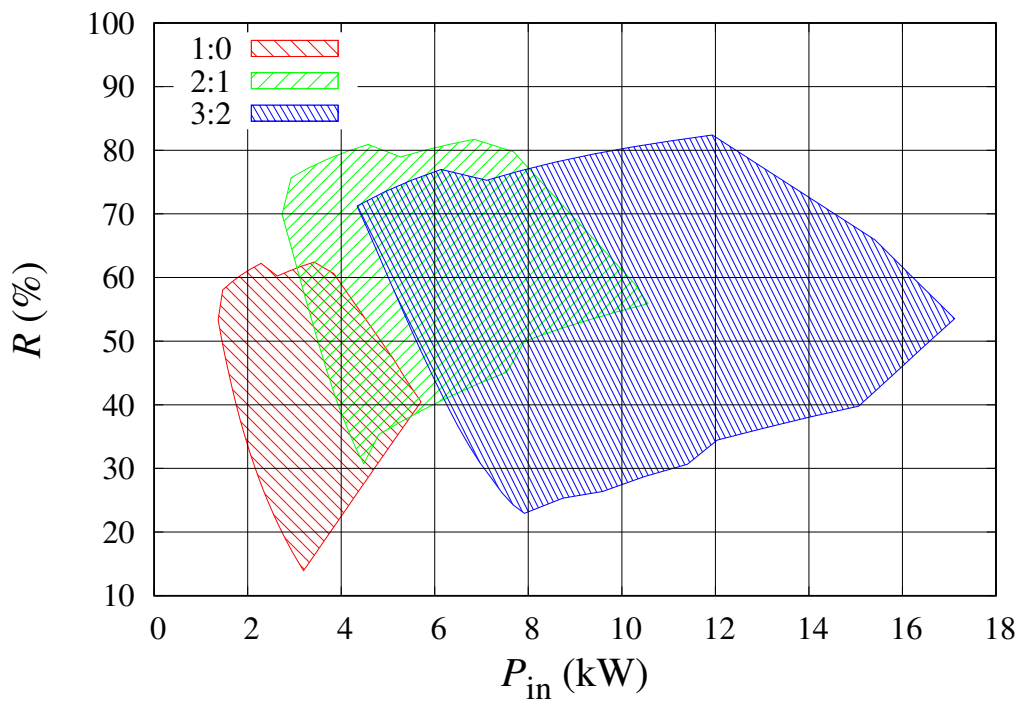


Figure 5. R for different BWRO configurations using sample 20 (Table 1) as C_f .

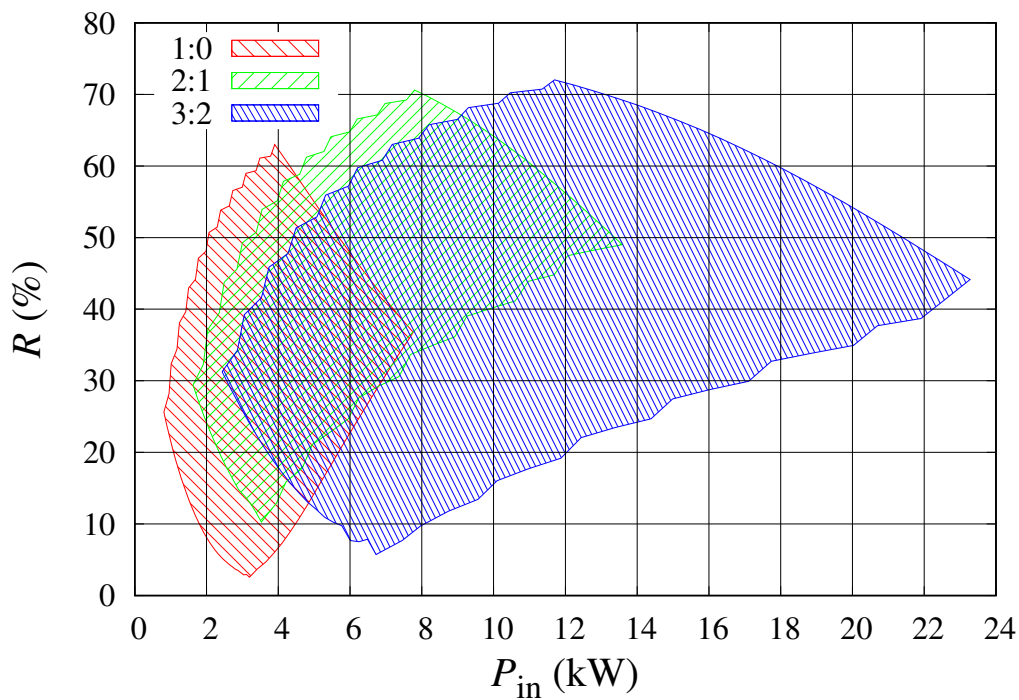


Figure 6. R for different BWRO configurations using sample 11 (Table 1) as C_f .

Figures 7 and 8 show the operating points that maximize Q_p for the BWRO configurations 1:0, 2:1 and 3:2, considering the C_f of samples 20 and 11, respectively. It can be observed that with higher C_f the curves are closer together and even intersect. Another factor affected by C_f is the appropriate P_{in} (for maximizing Q_p) range using each configuration. This range is notably lower for configurations 1:0 and 2:1. The operating curves of the 2:1 and 3:2 configurations are so close that a jump from 1:0

to 3:2 can be made directly depending on the trend of P_{in} . It can be observed that the curves are longer for the feedwater with higher C_f than for sample 20 (lower C_f). This is because at lower C_f , SWMMs produce more Q_p and are more likely to not meet the Q_{r-min} constraint or exceed the Q_{p-max} per SWMM. The BWRO system operation with higher C_f allows a wider operating range without exceeding the imposed constraints but producing a lower Q_p with the same P_{in} .

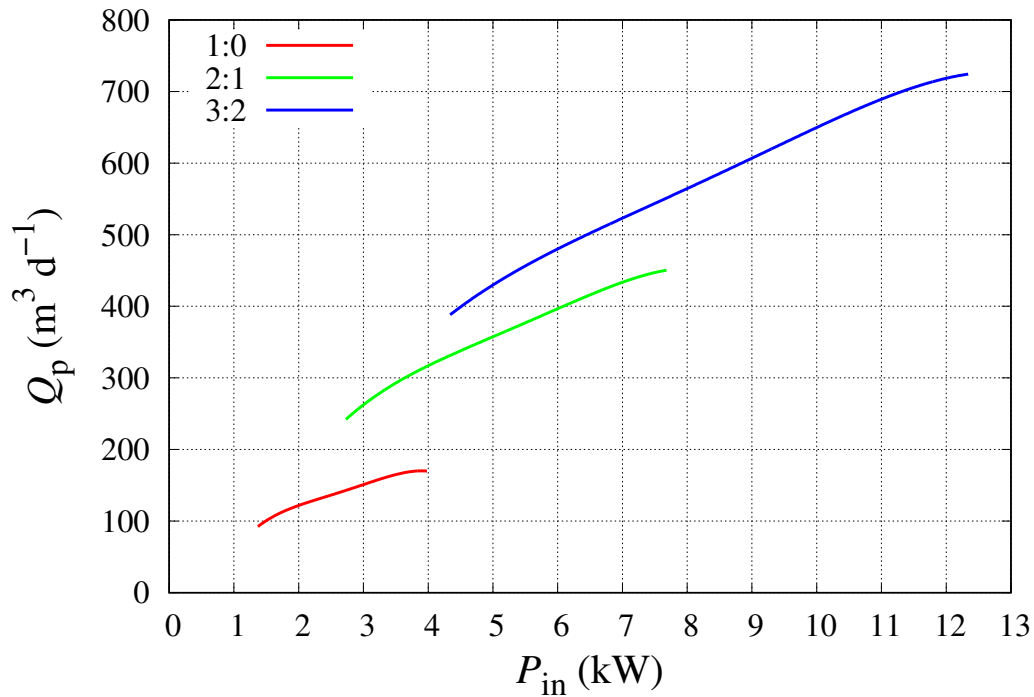


Figure 7. Curves of maximum Q_p for different BWRO configurations using sample 20 (Table 1) as C_f .

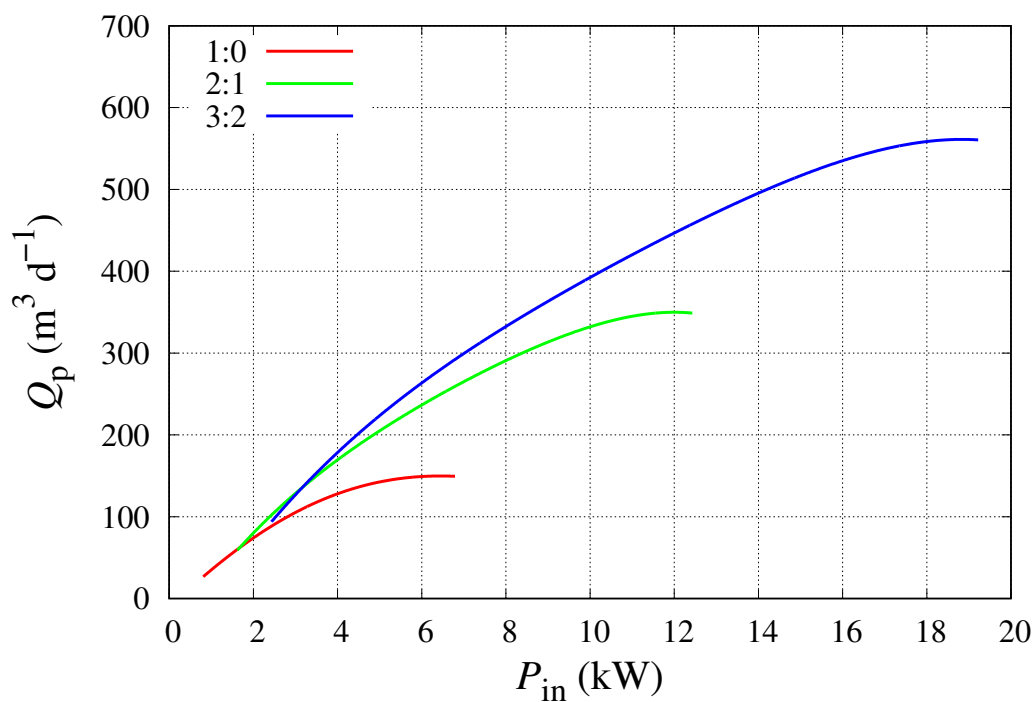


Figure 8. Curves of maximum Q_p for different BWRO configurations using sample 11 (Table 1) as C_f .

Table 2 shows the range of P_{in} in which each BWRO configuration should be applied considering five samples (20, 5, 22, 3 and 11 (Table 1)) representing different C_f of the studied groundwater well. Some overlap was considered in P_{in} to avoid excessive configuration changes, depending on the P_{in} trend (increasing or decreasing). It should be mentioned that some operating points that were very close to the constraints established by the membrane manufacturer were removed to avoid instabilities in the operation of the BWRO system. This is the main reason why higher P_{in} was required for lower C_f in addition to the selected p_f and Q_f steps that eliminate some possible operating points. The P_{in} required depends, among other things, on the osmotic pressure of the feed solution, which in turn not only depends on the amount of TDS but on its inorganic composition. Table 3 shows the R range for each configuration. These values are important as the reference for the on/off percentages of the RO concentrate valve (Figure 1). The data of the operating points for maximizing Q_p using configurations 1:0, 2:1 and 3:2 for the five samples shown in Tables 2 and 3 can be found in Appendix A.

Table 2. P_{in} (kW) range for different BWRO configurations and five C_f (samples 20, 5, 22, 3 and 11 (Table 1)).

Configuration	C_f (g L ⁻¹)				
	1.2	2.99	3.48	4.5	5.82
1 : 0	1.37–2.89	1.13–2.4	1.13–2.4	0.89–1.93	0.81–2.07
2 : 1	2.73–4.57	2.26–3.71	2.26–3.71	1.78–2.90	1.91–3.39
3 : 2	4.34–12.34	3.39–15.36	3.39–17.26	2.67–17	3.05–19.22

Table 3. R (%) range for different BWRO configurations and five C_f (samples 20, 5, 22, 3 and 11 (Table 1)).

Configuration	C_f (g L ⁻¹)				
	1.2	2.99	3.48	4.5	5.82
1 : 0	53.32–61.02	43.13–59.88	43.34–60.17	35.66–50.60	25.64–50.71
2 : 1	69.92–80.91	52.28–66.78	52.45–66.96	41.58–52.85	32.27–50.76
3 : 2	71.22–79.77	55.68–66.82	55.82–58.11	43.99–61.13	39.22–56.44

4. Conclusions

Operating a BWRO system is far from simple and acquires greater complexity under variable conditions of C_f (usual for groundwater sources) and P_{in} (for example when the BWRO is powered by renewable energy sources). An on-off control strategy based on simulations is presented in this work considering a BWRO system with a 3:2 configuration that is able to operate with other configurations (1:0, 2:0, 3:0, 2:1 and 3:1) depending on the P_{in} available. The operating points of each configuration that maximize Q_p for each P_{in} were considered. The simulations showed that only the 1:0, 2:1 and 3:2 configurations were of interest in the studied case. Depending on the variation of C_f and the Q_f available from the source, larger BWRO systems are possible with a wider range of possible configurations. It was found that with higher C_f there was closer concordance between the SOWs for the different configurations considered. Lower C_f values allowed the BWRO system to produce more permeate water with a wider operating range for the 1:0, 2:1 and 3:2 configurations. In future works, high pressure pump performances and the modelling and control of variable frequency drives and RO concentrate valves should be considered to obtain more accurate results in the operation of this type of system under variable operating conditions. Permeate quality constraints were not considered in this study as the water product was assumed to be for agricultural irrigation. Consideration of a maximum C_p would also be of interest in terms of its impact on SOWs and suitable operating ranges.

Author Contributions: Formal analysis, A.R.-G.; investigation, A.R.-G.; writing—original draft preparation, A.R.-G.; writing—review and editing, A.R.-G. and I.N.; supervision, I.N. All authors have read and agreed to the published version of the manuscript.

Funding: This research was not funded.

Conflicts of Interest: The authors declare no conflict of interest.

Abbreviations

The following abbreviations are used in this manuscript:

Nomenclature

<i>A</i>	Average water permeability coefficient ($\text{m d}^{-1} \text{bar}^{-1} \text{cm}^2$)
<i>B</i>	Average ion permeability coefficient (m d^{-1})
BWRO	Brackish water reverse osmosis
<i>C</i>	Concentration (mg L^{-1})
<i>Cond</i>	Conductivity ($\mu\text{S cm}^{-1}$)
<i>FF</i>	Flow factor
<i>n</i>	Number of membrane elements in series
P_{in}	Input power (kW)
PID	Proportional-integral-derivative
PV	Pressure vessel
<i>p</i>	Pressure (bar)
<i>Q</i>	Flow ($\text{m}^3 \text{d}^{-1}$)
<i>R</i>	Flow recovery (%)
RO	Reverse osmosis
<i>SEC</i>	Specific energy consumption (kWh m^{-3})
<i>SDI</i>	Silt density index
SOW	Safe operating window
SWMM	Spiral wound membrane module
<i>T</i>	Temperature
<i>TCF</i>	Temperature correction factor
<i>TDS</i>	Total dissolved solids
<i>Y</i>	Fraction recovery
Greek letters	
π	Osmotic pressure (bar)
Subscripts	
<i>b</i>	Brine
<i>f</i>	Feed
<i>i</i>	Membrane element <i>i</i>
<i>j</i>	Ion <i>j</i>
max	Maximum
min	Minimum
<i>p</i>	Permeate
<i>r</i>	Rejection

Appendix A. Operating Conditions for Maximizing Q_p Considering Three Bwro Configurations and Five Different Feedwater Samples

Table A1. P_{in} , p_f , Q_f and R for maximizing Q_p considering three different BWRO configurations and using samples 20 and 5 (Table 1) as feedwater.

Configuration	Sample 20				Sample 5			
	P_{in} (kW)	p_f (bar)	Q_f (m ³ d ⁻¹)	R (%)	P_{in} (kW)	p_f (bar)	Q_f (m ³ d ⁻¹)	R (%)
1:0	1.37	7.0	172	53.32	1.13	7.0	142	43.13
	1.46	7.5	172	58.04	1.21	7.5	142	47.51
	1.65	8.0	182	59.26	1.38	8.0	152	49.05
	1.85	8.5	192	60.36	1.56	8.5	162	50.41
	2.06	9.0	202	61.34	1.66	9.0	162	54.10
	2.29	9.5	212	62.22	1.86	9.5	172	55.12
	2.63	10.0	232	60.22	2.07	10.0	182	56.05
	2.89	10.5	242	61.02	2.17	10.5	182	59.19
	3.15	11.0	252	61.76	2.40	11.0	192	59.88
	3.42	11.5	262	62.43	2.64	11.5	202	60.51
	3.84	12.0	282	60.61	2.75	12.0	202	63.24
	3.98	12.0	292	58.27	3.01	12.5	212	63.70
					3.28	13.0	222	64.13
					3.40	13.5	222	66.50
					3.69	14.0	232	66.81
					3.85	14.0	242	64.87
					4.01	14.0	252	62.93
					4.16	14.0	262	61.01
					4.32	14.0	272	59.11
					4.48	14.0	282	57.24
				4.64	14.0	292	55.42	
				4.80	14.0	302	53.64	
				4.96	14.0	312	51.90	
				5.12	14.0	322	50.21	
				5.28	14.0	332	48.57	
2:1	2.73	7.0	344	69.92	2.26	7.0	284	52.28
	2.93	7.5	344	75.69	2.42	7.5	284	57.63
	3.31	8.0	364	77.24	2.76	8.0	304	59.60
	3.71	8.5	384	78.61	3.13	8.5	324	61.36
	4.13	9.0	404	79.83	3.31	9.0	324	65.45
	4.57	9.5	424	80.91	3.71	9.5	344	66.78
	5.27	10.0	464	78.96	4.13	10.0	364	67.98
	5.77	10.5	484	79.97	4.34	10.5	364	71.13
	6.29	11.0	504	80.89	4.80	11.0	384	72.06
	6.84	11.5	524	81.72	5.28	11.5	404	72.90
	7.68	12.0	564	79.76	5.50	12.0	404	75.36
					6.02	12.5	424	76.02
					6.55	13.0	444	76.63
					6.81	13.5	444	78.57
					7.38	14.0	464	79.06
					7.69	14.0	484	77.72
					8.01	14.0	504	76.21
					8.33	14.0	524	74.55
					8.65	14.0	544	72.74
					8.97	14.0	564	70.79
				9.28	14.0	584	68.72	
				9.60	14.0	604	66.55	
	4.34	7.0	546	71.22	3.39	7.0	426	55.68
	4.91	7.5	576	73.38	3.63	7.5	426	60.78
	5.50	8.0	606	75.29	4.14	8.0	456	62.79

Table A1. Cont.

Configuration	Sample 20				Sample 5			
	P_{in} (kW)	p_f (bar)	Q_f (m ³ d ⁻¹)	R (%)	P_{in} (kW)	p_f (bar)	Q_f (m ³ d ⁻¹)	R (%)
3:2	6.14	8.5	636	76.98	4.69	8.5	486	64.58
	7.11	9.0	696	75.28	4.97	9.0	486	68.32
	7.83	9.5	726	76.79	5.57	9.5	516	69.67
	8.58	10.0	756	78.14	6.20	10.0	546	70.88
	9.37	10.5	786	79.36	6.87	10.5	576	71.99
	10.19	8.5	816	80.47	7.19	11.0	576	74.60
	11.05	11.5	846	81.48	7.91	11.5	606	75.45
	11.94	12.0	876	82.39	8.67	12.0	636	76.24
	12.34	12.0	906	79.77	9.45	12.5	666	76.97
					10.27	13.0	696	77.63
					11.13	13.5	726	78.25
					11.54	14.0	726	79.97
					12.02	14.0	756	78.82
					12.49	14.0	786	77.53
					12.97	14.0	816	76.09
					13.45	14.0	846	74.50
					13.92	14.0	876	72.77
					14.40	14.0	906	70.90
				14.88	14.0	936	68.92	
				15.36	14.0	966	66.82	

Table A2. P_{in} , p_f , Q_f and R for maximizing Q_p considering three different BWRO configurations and using samples 22 and 3 (Table 1) as feedwater.

Configuration	Sample 22				Sample 3			
	P_{in} (kW)	p_f (bar)	Q_f (m ³ d ⁻¹)	R (%)	P_{in} (kW)	p_f (bar)	Q_f (m ³ d ⁻¹)	R (%)
1:0	1.13	7.0	142	43.34	0.89	7.0	112	35.66
	1.21	7.5	142	47.74	1.04	7.5	122	37.82
	1.38	8.0	152	49.28	1.20	8.0	132	39.72
	1.56	8.5	162	50.66	1.27	8.5	132	43.60
	1.66	9.0	162	54.35	1.45	9.0	142	45.05
	1.86	9.5	172	55.39	1.53	9.5	142	48.49
	2.07	10.0	182	56.32	1.73	10.0	152	49.60
	2.17	10.5	182	59.47	1.93	10.5	162	50.60
	2.40	11.0	192	60.17	2.02	11.0	162	53.51
	2.64	11.5	202	60.81	2.25	11.5	172	54.28
	2.75	12.0	202	63.52	2.34	12.0	172	56.90
	3.01	12.5	212	64.00	2.58	12.5	182	57.49
	3.28	13.0	222	64.43	2.69	13.0	182	59.85
	3.40	13.5	222	66.80	2.94	13.5	192	60.30
	3.56	13.5	232	64.83	3.05	14.0	192	62.43
	3.71	13.5	242	62.85	3.33	14.5	202	62.77
	3.86	13.5	252	60.89	3.61	15.0	212	63.08
	4.02	13.5	262	58.95	3.73	15.5	212	64.96
	4.17	13.5	272	57.05	3.91	15.5	222	63.36
	4.32	13.5	282	55.19	4.08	15.5	232	61.73
4.48	13.5	292	53.38	4.26	15.5	242	60.10	
				4.43	15.5	252	58.47	
				4.61	15.5	262	56.84	
				4.79	15.5	272	55.24	
				4.96	15.5	282	53.65	
				5.14	15.5	292	52.09	
				5.31	15.5	302	50.56	
				5.49	15.5	312	49.06	
				5.67	15.5	322	47.59	

Table A2. Cont.

Configuration	Sample 22				Sample 3			
	P_{in} (kW)	p_f (bar)	Q_f (m ³ d ⁻¹)	R (%)	P_{in} (kW)	p_f (bar)	Q_f (m ³ d ⁻¹)	R (%)
2:1	2.26	7.0	284	52.45	1.78	7.0	224	41.58
	2.42	7.5	284	57.79	2.08	7.5	244	44.18
	2.76	8.0	304	59.78	2.40	8.0	264	46.51
	3.13	8.5	324	61.55	2.55	8.5	264	51.04
	3.31	9.0	324	65.62	2.90	9.0	284	52.85
	3.71	9.5	344	66.96	3.06	9.5	284	56.66
	4.13	10.0	364	68.17	3.45	10.0	304	58.08
	4.34	10.5	364	71.29	3.86	10.5	324	59.37
	4.80	11.0	384	72.23	4.05	11.0	324	62.40
	5.54	11.5	424	71.19	4.49	11.5	344	63.43
	6.05	12.0	444	72.03	4.69	12.0	344	66.01
	6.87	12.5	484	70.87	5.17	12.5	364	66.84
	7.44	13.0	504	71.64	5.37	13.0	364	69.03
	8.03	13.5	524	72.35	5.89	13.5	384	69.70
	8.34	13.5	544	70.38	6.10	14.0	384	71.58
	8.65	13.5	564	68.28	6.65	14.5	404	72.14
	8.95	13.5	584	66.08	7.22	15.0	424	72.66
					7.46	15.5	424	74.22
					7.81	15.5	444	73.14
					8.17	15.5	464	71.95
				8.52	15.5	484	70.66	
				8.87	15.5	504	69.26	
				9.22	15.5	524	67.76	
				9.57	15.5	544	66.15	
				9.93	15.5	564	64.46	
				10.28	15.5	584	62.68	
				10.63	15.5	604	60.82	
				10.98	15.5	624	58.91	
3:2	3.39	7.0	426	55.82	2.67	7.0	336	43.99
	3.63	7.5	426	60.91	3.12	7.5	366	46.70
	4.14	8.0	456	62.92	3.60	8.0	396	49.12
	4.69	8.5	486	64.73	3.82	8.5	396	53.51
	4.97	9.0	486	68.44	4.35	9.0	426	55.38
	5.57	9.5	516	69.79	4.60	9.5	426	58.99
	6.20	10.0	546	71.02	5.18	10.0	456	60.46
	6.87	10.5	576	72.13	5.79	10.5	486	61.79
	7.94	11.0	636	71.39	6.07	11.0	486	64.60
	8.70	11.5	666	72.39	6.74	11.5	516	65.67
	9.89	12.0	726	71.51	7.03	12.0	516	68.02
	10.73	12.5	756	72.41	7.75	12.5	546	68.89
	12.04	13.0	816	71.44	8.06	13.0	546	70.87
	12.97	13.5	846	72.26	8.83	13.5	576	71.58
	17.26	14.0	1086	58.11	9.16	14.0	576	73.25
					9.98	14.5	606	73.84
					10.83	15.0	636	74.40
					11.19	15.5	636	75.78
					11.72	15.5	666	74.92
					12.25	15.5	696	73.97
				12.78	15.5	726	72.93	
				13.30	15.5	756	71.79	
				13.83	15.5	786	70.55	
				14.36	15.5	816	69.21	
				14.89	15.5	846	67.77	
				15.42	15.5	876	66.24	
				15.94	15.5	906	64.62	
				16.47	15.5	936	62.91	
				17.00	15.5	966	61.13	

Table A3. P_{in} , p_f , Q_f and R for maximizing Q_p considering three different BWRO configurations and using sample 11 (Table 1) as feedwater.

Configuration	P_{in} (kW)	p_f (bar)	Q_f (m ³ d ⁻¹)	R (%)
1:0	0.81	7.0	102	25.64
	0.95	7.5	112	28.21
	1.02	8.0	112	32.38
	1.18	8.5	122	34.40
	1.25	9.0	122	38.10
	1.42	9.5	132	39.67
	1.50	10.0	132	42.96
	1.69	10.5	142	44.19
	1.77	11.0	142	47.12
	1.98	11.5	152	48.08
	2.07	12.0	152	50.71
	2.30	12.5	162	51.47
	2.39	13.0	162	53.83
	2.64	13.5	172	54.42
	2.73	14.0	172	56.56
	3.00	14.5	182	57.03
	3.10	15.0	182	58.97
	3.38	15.5	192	59.33
	3.49	16.0	192	61.10
	3.78	16.5	202	61.38
	3.90	17.0	202	63.00
	4.09	17.0	212	61.63
	4.29	17.0	222	60.24
	4.48	17.0	232	58.83
	4.67	17.0	242	57.41
	4.86	17.0	252	55.99
	5.06	17.0	262	54.58
	5.25	17.0	272	53.17
	5.44	17.0	282	51.78
	5.64	17.0	292	50.40
5.83	17.0	302	49.04	
6.02	17.0	312	47.70	
6.22	17.0	322	46.39	
6.41	17.0	332	45.09	
6.60	17.0	342	43.83	
6.79	17.0	352	42.59	
2:1	1.62	7.0	204	29.41
	1.91	7.5	224	32.27
	2.03	8.0	224	37.17
	2.35	8.5	244	39.48
	2.49	9.0	244	43.74
	2.85	9.5	264	45.59
	3.00	10.0	264	49.28
	3.39	10.5	284	50.76
	3.55	11.0	284	53.93
	3.97	11.5	304	55.13
	4.14	12.0	304	57.87
	4.60	12.5	324	58.85
	4.78	13.0	324	61.22
	5.27	13.5	344	62.03
	5.47	14.0	344	64.09
	5.99	14.5	364	64.77
	6.20	15.0	364	66.57
	6.76	15.5	384	67.15
6.98	16.0	384	68.73	
7.57	16.5	404	69.22	

Table A3. Cont.

Configuration	P_{in} (kW)	p_f (bar)	Q_f (m ³ d ⁻¹)	R (%)
	7.80	17.0	404	70.61
	8.18	17.0	424	69.67
	8.57	17.0	444	68.65
	8.96	17.0	464	67.54
	9.34	17.0	484	66.36
	9.73	17.0	504	65.10
	10.11	17.0	524	63.77
	10.50	17.0	544	62.36
	10.89	17.0	564	60.87
	11.27	17.0	584	59.32
	11.66	17.0	604	57.71
	12.04	17.0	624	56.05
	12.43	17.0	644	54.34
	2.43	7.0	306	31.26
	2.86	7.5	336	34.26
	3.05	8.0	336	39.22
	3.53	8.5	366	41.63
	3.74	9.0	366	45.86
	4.27	9.5	396	47.77
	4.50	10.0	396	51.36
	5.08	10.5	426	52.90
	5.32	11.0	426	55.93
	5.95	11.5	456	57.18
	6.21	12.0	456	59.76
	6.90	12.5	486	60.80
	7.17	13.0	486	63.02
	7.91	13.5	516	63.87
	8.20	14.0	516	65.78
	8.99	14.5	546	66.50
	9.30	15.0	546	68.16
3:2	10.14	15.5	576	68.77
	10.46	16.0	576	70.22
	11.35	16.5	606	70.75
	11.70	17.0	606	72.03
	12.28	17.0	636	71.24
	12.86	17.0	666	70.39
	13.43	17.0	696	69.47
	14.01	17.0	726	68.49
	14.59	17.0	756	67.43
	15.17	17.0	786	66.31
	15.75	17.0	816	65.11
	16.33	17.0	846	63.83
	16.91	17.0	876	62.48
	17.49	17.0	906	61.07
	18.07	17.0	936	59.59
	18.65	17.0	966	58.05
	19.22	17.0	996	56.44

References

1. Qasim, M.; Badrelzaman, M.; Darwish, N.N.; Darwish, N.A.; Hilal, N. Reverse osmosis desalination: A state-of-the-art review. *Desalination* **2019**, *459*, 59–104. [\[CrossRef\]](#)
2. Karabelas, A.; Koutsou, C.; Kostoglou, M.; Sioutopoulos, D. Analysis of specific energy consumption in reverse osmosis desalination processes. *Desalination* **2018**, *431*, 15–21. [\[CrossRef\]](#)
3. Nassrullah, H.; Anis, S.F.; Hashaikh, R.; Hilal, N. Energy for desalination: A state-of-the-art review. *Desalination* **2020**, *491*, 114569. [\[CrossRef\]](#)

4. Kurihara, M.; Takeuchi, H. SWRO-PRO System in “Mega-ton Water System” for Energy Reduction and Low Environmental Impact. *Water* **2018**, *10*, 48. [[CrossRef](#)]
5. Voutchkov, N. Energy use for membrane seawater desalination—Current status and trends. *Desalination* **2018**, *431*, 2–14. [[CrossRef](#)]
6. Park, H.G.; Kwon, Y.N. Long-Term Stability of Low-Pressure Reverse Osmosis (RO) Membrane Operation—A Pilot Scale Study. *Water* **2018**, *10*, 93. [[CrossRef](#)]
7. Zhao, D.L.; Japip, S.; Zhang, Y.; Weber, M.; Maletzko, C.; Chung, T.S. Emerging thin-film nanocomposite (TFN) membranes for reverse osmosis: A review. *Water Res.* **2020**, *173*, 115557. [[CrossRef](#)]
8. Saleem, H.; Zaidi, S.J. Nanoparticles in reverse osmosis membranes for desalination: A state of the art review. *Desalination* **2020**, *475*, 114171. [[CrossRef](#)]
9. Ruiz-García, A.; Nuez, I. Performance Assessment of SWRO Spiral-Wound Membrane Modules with Different Feed Spacer Dimensions. *Processes* **2020**, *8*, 692. [[CrossRef](#)]
10. Okamoto, Y.; Lienhard, J.H. How RO membrane permeability and other performance factors affect process cost and energy use: A review. *Desalination* **2019**, *470*, 114064. [[CrossRef](#)]
11. Ruiz-García, A.; de la Nuez Pestana, I. Feed Spacer Geometries and Permeability Coefficients. Effect on the Performance in BWRO Spiral-Wound Membrane Modules. *Water* **2019**, *11*, 152. [[CrossRef](#)]
12. Anis, S.F.; Hashaikheh, R.; Hilal, N. Reverse osmosis pretreatment technologies and future trends: A comprehensive review. *Desalination* **2019**, *452*, 159–195. [[CrossRef](#)]
13. Li, Y.; Yang, S.; Zhang, K.; Bart Van der Bruggen. Thin film nanocomposite reverse osmosis membrane modified by two dimensional laminar MoS₂ with improved desalination performance and fouling-resistant characteristics. *Desalination* **2019**, *454*, 48–58. [[CrossRef](#)]
14. Li, S.; Cai, Y.H.; Schäfer, A.I.; Richards, B.S. Renewable energy powered membrane technology: A review of the reliability of photovoltaic-powered membrane system components for brackish water desalination. *Appl. Energy* **2019**, *253*, 113524. [[CrossRef](#)]
15. Joseph, A.; Damodaran, V. Dynamic simulation of the reverse osmosis process for seawater using LabVIEW and an analysis of the process performance. *Comput. Chem. Eng.* **2019**, *121*, 294–305. [[CrossRef](#)]
16. Rivas-Perez, R.; Sotomayor-Moriano, J.; Pérez-Zuñiga, G.; Soto-Angles, M.E. Real-Time Implementation of an Expert Model Predictive Controller in a Pilot-Scale Reverse Osmosis Plant for Brackish and Seawater Desalination. *Appl. Sci.* **2019**, *9*, 2932. [[CrossRef](#)]
17. Alatiqi, I.; Ghabris, A.; Ebrahim, S. System identification and control of reverse osmosis desalination. *Desalination* **1989**, *75*, 119–140. [[CrossRef](#)]
18. Robertson, M.; Watters, J.; Desphande, P.; Assef, J.; Alatiqi, I. Model based control for reverse osmosis desalination processes. *Desalination* **1996**, *104*, 59–68. [[CrossRef](#)]
19. Assef, J.Z.; Watters, J.C.; Deshpande, P.B.; Alatiqi, I.M. Advanced control of a reverse osmosis desalination unit. *J. Process Contr.* **1997**, *7*, 283–289. [[CrossRef](#)]
20. Abbas, A. Model predictive control of a reverse osmosis desalination unit. *Desalination* **2006**, *194*, 268–280. [[CrossRef](#)]
21. Gambier, A.; Wellenreuther, A.; Badreddin, E. Control system design of reverse osmosis plants by using advanced optimization techniques. *Desalin. Water Treat.* **2009**, *10*, 200–209. [[CrossRef](#)]
22. Bartman, A.R.; Christofides, P.D.; Cohen, Y. Nonlinear Model-Based Control of an Experimental Reverse-Osmosis Water Desalination System. *Ind. Eng. Chem. Res.* **2009**, *48*, 6126–6136. [[CrossRef](#)]
23. McFall, C.W.; Christofides, P.D.; Cohen, Y.; Davis, J.F. Fault-tolerant control of a reverse osmosis desalination process. *IFAC Proc. Vol.* **2007**, *40*, 161–166. [[CrossRef](#)]
24. Kim, G.; Park, J.; Kim, J.; Lee, H.; Heo, H. PID control of Reverse Osmosis desalination plant using Immune-Genetic Algorithm. In Proceedings of the 2009 ICCAS-SICE, Fukuoka, Japan, 18–21 August 2009; pp. 2977–2981.
25. Bartman, A.R.; McFall, C.W.; Christofides, P.D.; Cohen, Y. Model-predictive control of feed flow reversal in a reverse osmosis desalination process. *J. Process Contr.* **2009**, *19*, 433–442. [[CrossRef](#)]
26. Bartman, A.R.; Zhu, A.; Christofides, P.D.; Cohen, Y. Minimizing energy consumption in reverse osmosis membrane desalination using optimization-based control. *J. Process Contr.* **2010**, *20*, 1261–1269. [[CrossRef](#)]
27. Al-haj, M.A.; Ajbar, A.; Ali, E.; Alhumaizi, K. Robust model-based control of a tubular reverse-osmosis desalination unit. *Desalination* **2010**, *255*, 129–136. [[CrossRef](#)]

28. Emad, A.; Ajbar, A.; Almutaz, I. Periodic control of a reverse osmosis desalination process. *J. Process Contr.* **2012**, *22*, 218–227. [[CrossRef](#)]
29. Gambier, A. Control of a Reverse Osmosis plant by using a robust PID design based on multi-objective optimization. In Proceedings of the 2011 50th IEEE Conference on Decision and Control and European Control Conference, Orlando, FL, USA, 12–15 December 2011; pp. 7045–7050.
30. AlDhaifallah, M.; Sassi, K.; Mujtaba, I. PID Control of Reverse Osmosis Based Desalination Process. In *Computer Aided Chemical Engineering, Proceedings of the 22nd European Symposium on Computer Aided Process Engineering*; Bogle, I.D.L., Fairweather, M., Eds.; Elsevier: Amsterdam, The Netherlands, 2012; Volume 30, pp. 812–816. [[CrossRef](#)]
31. Li, D.; Yang, N.; Niu, R.; Qiu, H.; Xi, Y. FPGA based QDMC control for reverse-osmosis water desalination system. *Desalination* **2012**, *285*, 83–90. [[CrossRef](#)]
32. Zhao, T.; Niu, R.; Su, M.; Anderson, T. Steady state and dynamic modeling of RO desalination modules and system using EES. In Proceedings of the 2011 IEEE International Conference on Robotics and Automation, Shanghai, China, 9–13 May 2011; pp. 1–4.
33. Sobana, S.; Panda, R. Modeling and control of reverse osmosis desalination process using centralized and decentralized techniques. *Desalination* **2014**, *344*, 243–251. [[CrossRef](#)]
34. Phuc, B.D.H.; You, S.S.; Lim, T.W.; Kim, H.S. Modified PID control with H_{∞} loop shaping synthesis for RO desalination plants. *Desalin. Water Treat.* **2016**, *57*, 25421–25434. [[CrossRef](#)]
35. Phuc, B.D.H.; You, S.S.; Lim, T.W.; Kim, H.S. Dynamical analysis and control synthesis of RO desalination process against water hammering. *Desalination* **2017**, *402*, 133–142. [[CrossRef](#)]
36. Feliu-Batlle, V.; Rivas-Perez, R.; Linares-Saez, A. Fractional Order Robust Control of a Reverse Osmosis Seawater Desalination Plant. *IFAC-PapersOnLine* **2017**, *50*, 14545–14550. [[CrossRef](#)]
37. Zebbar, M.; Messlem, Y.; Gouichiche, A.; Tadjine, M. Super-twisting sliding mode control and robust loop shaping design of RO desalination process powered by PV generator. *Desalination* **2019**, *458*, 122–135. [[CrossRef](#)]
38. Khiari, W.; Turki, M.; Belhadj, J. Power control strategy for PV/Wind reverse osmosis desalination without battery. *Control Eng. Pract.* **2019**, *89*, 169–179. [[CrossRef](#)]
39. Ruiz-García, A.; Ruiz-Saavedra, E. 80,000 h operational experience and performance analysis of a brackish water reverse osmosis desalination plant. Assessment of membrane replacement cost. *Desalination* **2015**, *375*, 81–88. [[CrossRef](#)]
40. Ruiz-García, A.; Nuez, I. Long-term intermittent operation of a full-scale BWRO desalination plant. *Desalination* **2020**, *489*, 114526. [[CrossRef](#)]
41. Hasnain, S.M.; Alajlan, S.A. Coupling of PV-powered RO brackish water desalination plant with solar stills. *Desalination* **1998**, *116*, 57–64. [[CrossRef](#)]
42. Gocht, W.; Sommerfeld, A.; Rautenbach, R.; Melin, T.; Eilers, L.; Neskakis, A.; Herold, D.; Horstmann, V.; Kabariti, M.; Muhaidat, A. Decentralized desalination of brackish water by a directly coupled reverse-osmosis-photovoltaic-system—A pilot plant study in Jordan. *Renew. Energy* **1998**, *14*, 287–292. [[CrossRef](#)]
43. Schäfer, A.; Remy, C.; Richards, B. Performance of a small solar-powered hybrid membrane system for remote communities under varying feedwater salinities. *Water Supply* **2004**, *4*, 233–243. [[CrossRef](#)]
44. Richards, B.; Capão, D.; Schäfer, A. Renewable Energy Powered Membrane Technology. 2. The Effect of Energy Fluctuations on Performance of a Photovoltaic Hybrid Membrane System. *Environ. Sci. Technol.* **2008**, *42*, 4563–4569. [[CrossRef](#)]
45. Richards, B.S.; Masson, L.; Schäfer, A.I. Impact of Feedwater Salinity on Energy Requirements of a Small-Scale Membrane Filtration System. In *Appropriate Technologies for Environmental Protection in the Developing World: Selected Papers from ERTEP 2007, July 17–19 2007, Ghana, Africa*; Yanful, E.K., Ed.; Springer: Dordrecht, The Netherlands, 2009; pp. 123–137. [[CrossRef](#)]
46. Khayet, M.; Essalhi, M.; Armenta-Déu, C.; Cojocar, C.; Hilal, N. Optimization of solar-powered reverse osmosis desalination pilot plant using response surface methodology. *Desalination* **2010**, *261*, 284–292. [[CrossRef](#)]
47. Qiblawey, H.; Banat, F.; Al-Nasser, Q. Performance of reverse osmosis pilot plant powered by Photovoltaic in Jordan. *Renew. Energy* **2011**, *36*, 3452–3460. [[CrossRef](#)]
48. Cherif, H.; Belhadj, J. Large-scale time evaluation for energy estimation of stand-alone hybrid photovoltaic–wind system feeding a reverse osmosis desalination unit. *Energy* **2011**, *36*, 6058–6067. [[CrossRef](#)]

49. Park, G.L.; Schäfer, A.I.; Richards, B.S. Renewable energy powered membrane technology: The effect of wind speed fluctuations on the performance of a wind-powered membrane system for brackish water desalination. *J. Membr. Sci.* **2011**, *370*, 34–44. [[CrossRef](#)]
50. Richards, B.S.; Park, G.L.; Pietzsch, T.; Schäfer, A.I. Renewable energy powered membrane technology: Brackish water desalination system operated using real wind fluctuations and energy buffering. *J. Membr. Sci.* **2014**, *468*, 224–232. [[CrossRef](#)]
51. Richards, B.S.; Park, G.L.; Pietzsch, T.; Schäfer, A.I. Renewable energy powered membrane technology: Safe operating window of a brackish water desalination system. *J. Membr. Sci.* **2014**, *468*, 400–409. [[CrossRef](#)]
52. Richards, B.S.; Capão, D.P.; Früh, W.G.; Schäfer, A.I. Renewable energy powered membrane technology: Impact of solar irradiance fluctuations on performance of a brackish water reverse osmosis system. *Sep. Purif. Technol.* **2015**, *156*, 379–390. [[CrossRef](#)]
53. Ruiz-García, A.; de la Nuez-Pestana, I. A computational tool for designing BWRO systems with spiral wound modules. *Desalination* **2018**, *426*, 69–77. [[CrossRef](#)]
54. Ruiz-García, A.; Carrascosa-Chisvert, M.D.; Mena, V.; Souto, R.M.; Santana, J.J.; Nuez, I. Groundwater Quality Assessment in a Volcanic Mountain Range (South of Gran Canaria Island, Spain). *Water* **2019**, *11*, 754. [[CrossRef](#)]
55. Ruiz-García, A.; Ruiz-Saavedra, E.; Báez, S.O.P. Evaluation of the first seven years operating data of a RO brackish water desalination plant in Las Palmas, Canary Islands, Spain. *Desalin. Water Treat.* **2015**, *54*, 3193–3199. [[CrossRef](#)]
56. Wijmans, J.; Baker, R. The solution-diffusion model: A review. *J. Membr. Sci.* **1995**, *107*, 1–21. [[CrossRef](#)]
57. Al-Obaidi, M.; Kara-Zaitri, C.; Mujtaba, I. Scope and limitations of the irreversible thermodynamics and the solution diffusion models for the separation of binary and multi-component systems in reverse osmosis process. *Comput. Chem. Eng.* **2017**, *100*, 48–79. [[CrossRef](#)]
58. Kucera, J. *Reverse Osmosis: Industrial Processes and Applications*; John Wiley & Sons: Hoboken, NJ, USA, 2015.
59. Ruiz-García, A.; Feo-García, J. Estimation of maximum water recovery in RO desalination for different feedwater inorganic compositions. *Desalin. Water Treat.* **2017**, *70*, 34–45. [[CrossRef](#)]
60. Solutions, D.W. *Filmtec Reverse Osmosis Membranes Technical Manual*; Dupont Water Solutions: Edina, MN, USA, 2020.



© 2020 by the authors. Licensee MDPI, Basel, Switzerland. This article is an open access article distributed under the terms and conditions of the Creative Commons Attribution (CC BY) license (<http://creativecommons.org/licenses/by/4.0/>).